THE JOURNAL OF PHYSICAL CHEMISTRY Letters

LETTER

pubs.acs.org/JPCL

Efficient Energy Transfer in Light-Harvesting Systems, III: The Influence of the Eighth Bacteriochlorophyll on the Dynamics and Efficiency in FMO

Jeremy Moix,[†,‡,∥] Jianlan Wu,[¶,∥] Pengfei Huo,[§] David Coker,[§,⊥] and Jianshu Cao*[,†,∥]

[†]Department of Chemistry, Massachusetts Institute of Technology, 77 Massachusetts Avenue, Cambridge, Massachusetts 02139, United States

[‡]School of Materials Science and Engineering, Nanyang Technological University, Singapore 639798,

[¶]Department of Physics, Zhejiang University, 38 ZheDa Road, Hangzhou, China 310027

[§]Department of Chemistry, Boston University, 590 Commonwealth Avenue, Boston, Massachusetts 02215, United States

[∥]Singapore−MIT Alliance for Research and Technology, 18 Medical Drive, Singapore 117456

[⊥]Complex Adaptive Systems Laboratory and School of Physics, University College Dublin, Dublin 4, Ireland

Supporting Information

ABSTRACT: The most recent crystal structure of the Fenna−Matthews−Olson (FMO) protein complex indicates the presence of an additional eighth chromophore, which has been proposed to serve as a link between the chlorosome and the remaining seven chromophores. Here, we investigate the implications of this scenario through numerical calculations with the generalized Bloch−Redfield (GBR) equation and the noninteracting blip approximation (NIBA). It is shown that the oscillations often observed in the population relaxation of sites 1 and 2 may be completely suppressed in the eight-site model due to the initial preparation. Second it is demonstrated that while the presence of the eighth chromophore does not cause a dramatic change in the energy-transfer efficiency, it does however lead to a dominant energy-transfer pathway that can be characterized by an effective three-site system. Finally, we confirm that the energy-transfer process in the eight-site complex remains efficient and robust through computations of the optimal values of the bath parameters.

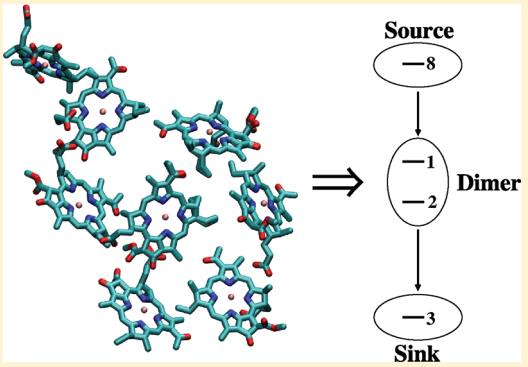

SECTION: Statistical Mechanics, Thermodynamics, Medium Effects

The Fenna−Matthews−Olson (FMO) protein is one of the simplest and most well studied light-harvesting systems. The protein complex exists as a trimer of three identical subunits whose function is to link the chlorosome antenna complex, where light harvesting takes place, with the reaction center, where charge separation occurs. FMO is also one of the earliest light-harvesting systems for which a high-resolution crystal structure has been obtained.[1] This early crystal structure indicated that each of the three FMO subunits contains seven Bacteriochlorophyll (Bchl) chromophores, which serve as the primary energy-transfer pathway between the chlorosome and the reaction center.[2−5] Recently, however, a more careful crystallographic analysis of FMO has been performed that demonstrates that the individual subunits contain eight Bchls, not seven.[6,7] The eighth Bchl resides on the surface of the protein complex, and it has been suggested that this additional chromophore is often lost during sample preparation.

From an energy-transfer perspective, the presence of an additional chromophore may challenge the current understanding of how exciton transfer occurs in FMO. For example, in many previous studies on the seven Bchl complex, it is thought that two nearly independent energy-transfer pathways exist.[8−11,13] Sites 1 and 6 are approximately equidistant from the antenna complex, and both are assumed to be possible locations for accepting the excitation from the chlorosome. From there, the energy is subsequently funneled either from site 1 to 2 (pathway 1) or from site 6 to sites 7, 5, and 4 (pathway 2). The terminal point through either route is site 3, where the exciton is then transferred to the reaction center (see Figure 1a). The couplings within each of the pathways are much larger than the couplings between the two, which implies that the two routes are nearly independent.[9,13,14] In the second paper of this series, the two pathways and the respective probability of traversing each have been quantified using a flux analysis.[13]

However, this two-pathway picture is not entirely consistent with the recent experimental data. The new crystal structure

Received: September 16, 2011
Accepted: November 14, 2011
Published: November 14, 2011

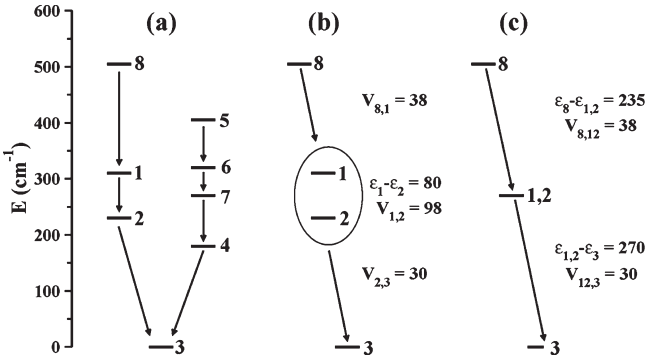

Figure 1. Energy diagrams for the eight-site model (a), the reduced four-site model (b), and the reduced three-site model (c) used in the calculations of Figure 3.

indicates that the eighth chromophore resides roughly midway between the baseplate and the Bchl at site 1.[6,7,15] Additionally, Renger and co-workers argued in ref 15 that the eighth Bchl provides the most efficient path for exciton injection into FMO as a result of its position and orientation with respect to the chlorosome. If this is correct and site 8 serves as the primary acceptor of excitation energy from the chlorosome, then a preferential energy-transfer route emerges through pathway 1. Due to the weak interpathway couplings, the secondary channel involving the remaining four chromophores in pathway 2 is largely bypassed in this scheme. This observation may have a significant impact on the efficiency and robustness of the energy-transfer process. The main objective of this work is to address this issue by exploring how the dynamics and the energy-transfer efficiency in FMO are affected by the presence of the eighth site and a realistic environment.

The first major conclusion of the present study is related to the population dynamics in FMO. In many of the previous studies of the seven-site model of FMO, the population relaxation dynamics are modeled with site 1 or site 6 initially populated.[8−12] Under either of these initial conditions, pronounced oscillations in the short-time dynamics are observed. However, when site 8 is initially excited,[15] the oscillations in the populations are completely suppressed. This lack of oscillations has been independently observed in the dynamics recently reported in refs 15−17. Here, we provide a simple explanation for this behavior. The eighth Bchl maintains a large energy gap with the other seven sites in FMO in order to facilitate efficient directed energy transport. However, it is also rather weakly coupled to the remaining Bchls. This leads to a slow incoherent decay of the initial population at site 8 and hence a broad distribution of initial conditions at the dimer. The consequence of this result is that the population oscillations generally observed between sites 1 and 2 are completely suppressed, which illustrates the importance of the initial conditions on the dynamics of the dimer.

The second key result of this work demonstrates that if the eighth Bchl is the primary acceptor of excitation energy from the chlorosome, as recently proposed, then a primary energy-transfer pathway in FMO does indeed emerge.[15] Note that this situation is substantially different from the previous interpretations of the energy flow in the seven site models where two independent pathways are generally assumed to exist. The extent of this effect and its impact on the energy-transfer efficiency is quantified by introducing reduced models of FMO that consist of only a subset of the sites in the full system. It is demonstrated that sites 8, 1, 2, and 3, which constitute pathway 1, provide the largest contribution to the dynamics of the full system. The remaining four sites of pathway 2 are seen to play a relatively small role. Despite the fact that only a single pathway dominates the energy-transfer process, we also show that the presence of the extra Bchl does not significantly impact the efficiency or robustness of FMO. The eight-site model leads to only a slight increase in the transfer time as compared with the seven-site system and thus maintains the same high efficiency as observed in previous studies of FMO.

Based upon energetic arguments, it has been suggested that the presence of the eighth Bchl leads to optimal energy transfer in FMO.[15] That is, its location near the chlorosome allows for a large coupling to the antenna complex as well as substantial overlap of the absorption spectrum of the eighth Bchl with the fluorescence spectrum of the chlorosome. These factors result in efficient transfer of the excitation energy into FMO while simultaneously allowing the eighth chromophore to maintain a large energy gap with the remaining Bchls and hence a favorable energy-transport landscape. These features implicitly suggest that there should be an optimal value of the site energy of the eighth Bchl. Here, it is demonstrated that this observation is correct. However, in this case, the behavior is independent of the presence of the chlorosome and can be understood by considering a further reduction of pathway 1 to only three sites. The result of this procedure is a downhill configuration of three more or less equally spaced sites (see Figure 1c), which is known to allow for highly efficient energy transfer.[18]

Recently, several studies have shown that the environment does not have an entirely destructive role in the energy-transport properties of excitonic systems.[11,13,19−22] Instead, the environment can serve to enhance both the efficiency and robustness of the energy-transfer process. Optimal values have been shown to exist for the temperature as well as other bath parameters, which maximize the energy-transfer efficiency in several light-harvesting systems. Moreover, the experimentally fitted model parameters for FMO are near-optimal in many cases. An extensive search for the optimal environmental parameters has been recently presented in refs 11 and 23. In addition to the above findings, we also explore the effect of the eighth Bchl on the environmentally assisted energy-transport properties in FMO. It is found that the optimal values of the bath parameters are similar to those found in the seven-site model but are closer to the experimental values in general. As has been observed before, the energy-transfer efficiency is relatively stable over a broad range of parameters, illustrating the robustness of the network.[11]

In the next paragraphs, we present the average trapping time formalism, which is used in the remainder of the discussion as a measure of the energy-transfer efficiency.[11,24] This is followed by a brief outline of the generalized Bloch−Redfield (GBR) approach and the model Hamiltonian for the eight-site FMO complex used in the numerical calculations. The results for the population dynamics and the development of the reduced models for FMO are discussed in the ensuing section. Calculations of the trapping time as a function of the site energies and bath parameters are then presented. There, it is demonstrated that optimal values exist for many of these parameters and additionally that the experimentally fitted values for FMO are near-optimal.

Average Trapping Time. The formalism for calculating the averaging trapping time in light-harvesting systems has been presented in detail previously in refs 11 and 18. Here, we provide only

the salient results. The total system is characterized by a discrete N-site system Hamiltonian, H_s, and its interaction with the environment, H_{sb}. Each site of the system is coupled to an independent bath of harmonic oscillators with the respective Hamiltonians, $H_b = (1/2)\Sigma_j(p_j^2 + \omega_j^2 x_j^2)$. The total Hamiltonian is then given by

$$H = \sum_n^N \varepsilon_n |n\rangle\langle n| + \sum_{n\neq m}^N V_{nm}|n\rangle\langle m| + \sum_n^N |n\rangle\langle n|[H_b^{(n)} + \sum_j c_j^{(n)} x_j^{(n)}] \quad (1)$$

where $c_j^{(n)}$ denotes the coupling coefficient of site n to the jth mode of its associated bath. The values of the site energies, ε_n, and coupling constants, V_{nm}, are specified below.

The time evolution of the reduced density matrix of this system can be conveniently described in the Liouville representation as

$$\frac{\partial\rho(t)}{\partial t} = -L_{tot}\rho(t) = -(L_s + L_{trap} + L_{decay} + L_{sb})\rho(t) \quad (2)$$

where $L_s\rho = i/\hbar[H_s,\rho]$ describes the coherent evolution under the bare system Hamiltonian H_s. In light-harvesting systems, the energy flows irreversibly to the reaction center, which is modeled here through the trapping operator $[L_{trap}]_{nm,nm} = (k_{t_m} + k_{t_n})/2$, where k_{t_n} denotes the trapping rate at site n. Notice that the trapping operator is a completely real quantity. As a result, it leads to pure exponential decay of the populations in eq 2. The energy transfer in FMO exhibits almost unit quantum yield. As a result, the decay rate of the excitation at any site to the ground state, k_d, is expected to be much smaller than the trapping rate, $k_t \gg k_d$. This allows for the simplification $L_{decay} = 0$.

Generalized Bloch−Redfield Equation. It remains to account for the Liouville operator describing the system−bath coupling L_{sb} in eq 2. For a harmonic bath linearly coupled to the system, the time correlation function of the bath coupling operators is given by the standard relation[25,26]

$$C(t) = \frac{1}{\pi}\int_0^\infty d\omega\, J(\omega)\left(\coth\left(\frac{\hbar\beta\omega}{2}\right)\cos(\omega t) - i\sin(\omega t)\right) \quad (3)$$

where $\beta = 1/k_B T$ and $J(\omega) = (\pi/2)\Sigma_j(c_j^2/\omega_j)\delta(\omega - \omega_j)$ is the spectral density of the bath. For simplicity, we assume that the spectral density is the same for each of the independent baths and given by the Drude form

$$J(\omega) = 2\lambda\omega_c\frac{\omega}{\omega^2 + \omega_c^2} \quad (4)$$

where λ is the bath reorganization energy and ω_c is the Debye cutoff frequency. For this special choice, the correlation function may be expanded in terms of the Matsubara frequencies, $\nu_j = (2\pi j/\hbar\beta)$, as[11,25,26]

$$C(t) = \left(\frac{2\lambda}{\hbar\beta} + \frac{4\lambda\omega_c}{\hbar\beta}\sum_{j=1}^\infty \frac{\omega_c}{\omega_c^2 - \nu_j^2} - i\lambda\omega_c\right)e^{-\omega_c t} - \frac{4\lambda\omega_c}{\hbar\beta}\sum_{j=1}^\infty \frac{\nu_j}{\omega_c^2 - \nu_j^2}e^{-\nu_j t} = \sum_{j=0}^\infty \alpha_j e^{-\nu_i t} \quad (5)$$

which defines the complex expansion coefficients α_j with the condition $\nu_0 = \omega_c$.

The dynamics in FMO have been computed using a variety of methods ranging in both accuracy and cost.[9,10,14,16,23,27] Here, we choose the approximate generalized Bloch−Redfield (GBR) method, which follows from a second-order cumulant expansion in the system−bath interaction. It provides an accurate but computationally friendly approach for the propagation of the density matrix over much of the physically relevant parameter space.[11,24] Due to the decomposition of the bath autocorrelation function in eq 5, the system−bath interaction may be accounted for through the introduction of auxiliary fields. The GBR equation of motion for the reduced density matrix is then given by

$$\frac{\partial\rho(t)}{\partial t} = -(L_{sys} + L_{trap})\rho(t) - i\sum_n^N\sum_{j=0}^\infty [A_n, g_{n,j}(t)] \quad (6)$$

The coupling of each Bchl to an independent bath leads to the additional sum over the N sites where the system operator $A_n = |n\rangle\langle n|$ and $g_{n,j}$ denotes the jth auxiliary field coupled to site n. The auxiliary variables are subject to the initial conditions $g_{n,j}(0) = 0$ and obey the equations of motion

$$\frac{\partial g_{n,j}(t)}{\partial t} = -(L_{sys} + L_{trap} + \nu_j)g_{n,j}(t) - i\,\mathrm{Re}(\alpha_j)[A_n,\rho(t)] + \mathrm{Im}(\alpha_j)[A_n,\rho(t)]_+ \quad (7)$$

where the plus subscript denotes anticommutation.

Trapping Time. The mean residence time at site n is, by definition

$$\langle\tau_n\rangle = \int_0^\infty dt\,\rho_{nn}(t) \quad (8)$$

where ρ_{nn} denotes the population at site n. The average trapping time is then given simply as the sum of the residence times at each of the N sites, $\langle t\rangle = \Sigma_{n=1}^N \langle\tau_n\rangle$. Invoking the steady-state solution of eq 2, $L_{tot}\langle t\rangle = \rho(0)$, then the average trapping time is given by the compact expression

$$\langle t\rangle = \mathrm{Tr}(L_{tot}^{-1}\rho(0)) \quad (9)$$

where the trace is taken over the site populations of the reduced density matrix.

Eight-Site FMO Model. The Hamiltonian for FMO is constructed from the crystal structure recently deposited in the protein data bank (pdb code: 3eoj).[7] The site energies are taken from those computed in ref 15, and the coupling element between sites n and m is calculated from the dipole−dipole approximation

$$V_{nm} = C\left(\frac{\mathbf{d}_n\cdot\mathbf{d}_m}{|\mathbf{r}_{nm}|^3} - 3\frac{(\mathbf{d}_n\cdot\mathbf{r}_{nm})(\mathbf{d}_m\cdot\mathbf{r}_{nm})}{|\mathbf{r}_{nm}|^5}\right) \quad (10)$$

Additional details and the explicit system Hamiltonian are given in the Supporting Information. Aside from the eighth site, the most significant difference between the present model Hamiltonian and the model previously derived by Cho et al.[28] is in the energy difference between sites 1 and 2. In the current case, the energy transfer through pathway 1 is entirely energetically favorable, whereas a barrier is present between sites 1 and 2 in the model of ref 28.

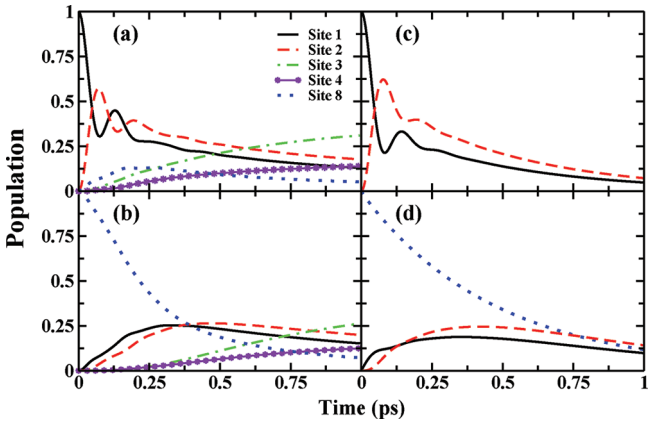

Figure 2. Site populations in the eight-site model of FMO calculated with the GBR when Bchl 1 (a) or 8 (b) is initially excited. The populations of the remaining sites 5, 6, and 7 are never larger than 10% and not shown. The site populations of the dimer are calculated using the NIBA of eq 11 (c) with site 1 initially excited and (d) with distributed initial conditions defined in 14. In all cases, the temperature is 300 K with a reorganization energy of 35 cm^{-1} and cutoff frequency of ω_c^{-1} = 50 fs.

Unless otherwise stated, the bath is characterized by the experimentally fitted values for the reorganization energy of 35 cm^{-1} and Debye frequency of ω_c^{-1} = 50 fs (105 cm^{-1}).[8,28] Additionally, the temperature is 300 K, and the trap is located at site 3 with a trapping rate of k_t = 1 ps^{-1}.

Population Dynamics and Suppression of the Oscillations. The time evolution of the populations in the eight-site model of FMO calculated from eq 2 using the GBR is shown in Figure 2a and b for the initial population located at site 1 and site 8, respectively. The bath parameters are taken at their fitted values specified above, and the trap at site 3 is not included. The most striking difference seen between Figures 2a and b is the absence of the oscillations in the populations of the dimer when site 8 is initially excited. Other recent studies of the eight-site model of FMO have also observed a similar lack of oscillations.[15−17] The origin of this effect may be traced to the initial conditions at the dimer. The energy difference between site 8 and the remaining sites is much larger than that of any of its respective couplings. This small coupling and large energy gap lead to the rather slow incoherent exponential relaxation of the population of site 8 seen in Figure 2b. The resulting initial conditions at sites 1 and 2 are then given by a corresponding incoherent distribution. It is this dephasing that suppresses the oscillations generally observed in the dynamics of the dimer.

By applying the noninteracting blip approximation (NIBA) to the spin-boson model, Pachon and Brumer established that a necessary condition for the presence of the oscillations in the dimer is an effective low temperature.[27] The results of Figure 2 demonstrate that the initial conditions impose an additional constraint on the observation of population oscillations. Note that there are a variety of other initial preparations, such as starting from an eigenstate of the total system or exciting the system with incoherent light,[29] which will also suppress the oscillations in the dimer.

In order to analyze the influence of the initial conditions in more detail, the dynamics of the dimer calculated using the NIBA are presented in Figures 2c and d. This approximation is equivalent to a second-order master equation in the polaron-transformed Hamiltonian,[25,31] and its validity for light-harvesting systems has been recently discussed in ref 27. The population dynamics described therein may be formulated as the generalized master equation[30−32]

$$\frac{\partial P_n(t)}{\partial t} = \int_0^t dt' \sum_{m=1}^{N} K_{nm}(t-t')P_m(t') \tag{11}$$

where $P_n(t)$ denotes the population of site n at time t. The elements of the time-dependent transition matrix are constructed in the standard fashion[33]

$$K_{nm}(t) = (1-\delta_{nm})W_{mn}(t) - \delta_{nm}\sum_k W_{nk}(t) \tag{12}$$

where δ_{nm} is the Kronecker delta function and the individual rate kernels are given by the NIBA

$$W_{nm}(t) = 2|V_{nm}^2|\mathrm{Re}\left[e^{i(\varepsilon_n-\varepsilon_m-2\lambda)t-2\int_0^t dt'\int_0^{t'}dt''C(t'')}\right] \tag{13}$$

As defined previously, the coupling between sites n and m is denoted by V_{nm}, ε_n is the energy of site n, λ is the reorganization energy, and $C(t)$ is the bath correlation function given in eq 5. The results shown in Figure 2c are calculated from eq 11 with the initial population located at site 1 and are seen to capture the key features of the full GBR dynamics shown in Figure 2a. The decay is accounted for by setting the transfer elements K_{n1} and K_{n2} to zero for all sites $n > 2$, which allows for population transfer from the dimer to the remaining Bchls but prevents any back-transfer. Effectively, this results in the addition of traps at sites 1 and 2 and thus leads to the population decay of the dimer. Without this decay, the two-site dynamics reproduce those of ref 27.

As has been alluded to previously, the lack of oscillations in the dimer when the initial population is located at site 8 may be explained by creating a distribution of initial conditions at site 1. All of the population is initially located at site 1 in Figure 2a, whereas in Figure 2b, the corresponding initial conditions are given by the population steadily flowing from site 8. This slow incoherent decay of the population at site 8 may be adequately fitted to the single exponential $P_8(t) = \exp(-\gamma t)$, where γ = 3 ps^{-1}. Assuming that site 8 decays only into site 1, the population of the latter is given by $1 - P_8(t)$, and the corresponding transition rate is $W_{81}(t) = \gamma\exp(-\gamma t)$. The influence of site 8 on the oscillatory behavior of the dimer can then be captured by convoluting the dynamics given in Figure 2c (denoted by $P_n(t)$) with this initial condition[34]

$$\bar{P}_n(t) = \int_0^t dt'\, P_n(t-t')W_{81}(t') \tag{14}$$

The result of this procedure is shown in Figure 2d. As is evident, the oscillatory behavior has completely disappeared. For large γ, the transition rate becomes a delta function, and the dynamics of Figure 2c are recovered. However, oscillations in the populations of both states can be observed only if the decay rate out of site 8 is increased 5-fold. The role of γ on the population dynamics of the dimer is shown in more detail in Figure 1 of the Supporting Information. The presence or absence of the trap simply effects the long-time decay of the dimer populations and is irrelevant for the short-time oscillatory behavior. These results demonstrate the importance of the initial preparation of the populations on the oscillations in the dynamics.

It should be noted that while the NIBA calculations lead to qualitatively similar population dynamics to those given by the GBR, neither of the two approaches are exact. In FMO and other

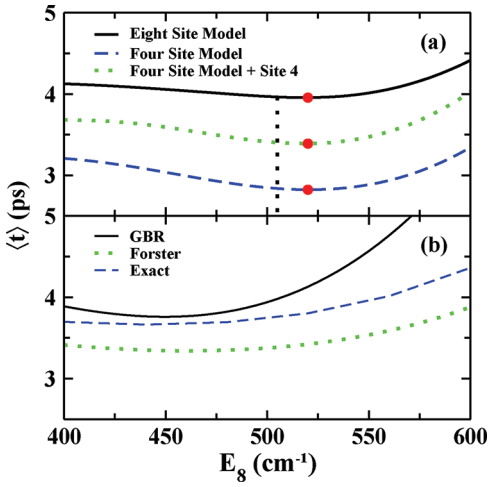

Figure 3. The trapping time as a function of the site energy of Bchl 8. The solid (black) line and dashed (blue) line in (a) correspond to the results calculated from the full eight-site model and with only the four sites of pathway 1, respectively. The dotted (green) line is the trapping time calculated from the four-site model with the addition of site 4. The red dots correspond to the optimal site energies, and the vertical dashed line indicates the fitted value of the site energy of Bchl 8 of 505 cm^{-1} determined in ref 15. Panel (b) contains results for the three-site model calculated with the GBR (solid black line), Förster theory (dotted green line), and hierarchical equation of motion (dashed blue line). The remaining parameters are the same as those in Figure 2.

light-harvesting systems, many of the model parameters are of the same order of magnitude. For instance, the couplings, V_{nm}, and energy differences, $\varepsilon_n - \varepsilon_m$, as well as the reorganization energy, λ, and thermal energy, β^{-1}, are all of comparable magnitude. As a result, methods based on second-order perturbation theory are, in general, insufficient to quantitatively describe the dynamics. A systematic procedure for computing higher-order contributions to the NIBA rates has been derived and recently implemented.[13,32] This leads to non-negligible corrections to the dynamics in the spin-boson model, FMO and LH2 (unpublished). Thus, while the results in Figure 2 and those of ref 27 capture the qualitative features that are necessary to analyze the energy- transfer behavior, there will be quantitative corrections from higher-order terms.

Pathway Analysis and the Ladder Configuration. Regardless of the presence or absence of oscillations, it is readily seen from Figures 2a and b that the population primarily flows through pathway 1. Among the sites in pathway 2, only site 4 ever accumulates more than 10% of the population. Particularly for times less than 500 fs, the sites from pathway 2 are scarcely populated. Similar behavior of the population dynamics has been seen in many other simulations of the seven-site model for FMO.[9,10,14−17] These observations lead to the first reduced model for FMO, which consists of only the four sites in pathway 1 shown in Figure 1b. As demonstrated below, this model is able to capture the key qualitative features of the energy-transfer process. One may proceed further by noting that sites 1 and 2 are coupled more strongly than the energy difference between the two. Additionally, sites 8 and 3 are widely separated from either site in the dimer. The couplings between the distant sites and dimer are also rather weak (see values in the model Hamiltonian in the Supporting Information and Figure 1b). As a result, there can be rapid coherent energy transfer between sites 1 and 2, whereas the transfer to sites 8 or 3 will be comparatively slow. Therefore, when the initial population is located at site 8, we may simply assume that these two sites of the dimer behave as one effective site with an energy that is the average of the two (270 cm^{-1}). A similar "mean state" idea for developing this type of reduced model has been suggested in ref 35, which explores the behavior of a dimer embedded in the PC645 photosynthetic network. Furthermore, the coupling between site 8 and the terminal site 3 is negligibly small. This leads to a three-site model for FMO where the couplings are determined by the nearest-neighbor values, as shown in Figure 1c.

Site Energy of Bchl 8. Figure 3 displays the average trapping time calculated as a function of the site energy of Bchl 8. It contains two additional key findings of this work. The first is that the trapping time behavior, and hence the efficiency, seen in the eight-site model of FMO is largely governed by the sites in pathway 1. The second feature is that an optimal value exists for the site energy of Bchl 8, and moreover, the optimum is near the fitted value determined in ref 15. The source of the latter is the highly efficient ladder configuration shown in Figure 1c.

Figure 3a displays the average trapping time calculated with the full Hamiltonian given in the Supporting Information along with the corresponding results for the four-site model of FMO (see Figures 1a and b). The bath parameters are taken at their experimentally fitted values with the temperature of 300 K. Figure 3b contains the results from the three-site model shown in Figure 1c. For this case, the exact trapping time calculated from the hierarchical equation of motion method is also presented, as well as the results of a Förster theory calculation. As can be seen, both the GBR and the Förster calculations predict optimal values of the site energy that semiquantitatively capture the behavior of the exact hierarchical results. The application of Förster theory to the dynamics in FMO (as well as higher-order corrections) is the focus of the second paper of this series.[13]

These results demonstrate that the energy transport is dominated by a subset of the sites in FMO and furthermore that the mechanism is correctly described by Förster theory. While the four-site model does not quantitatively capture the trapping time results of the full eight-site system, it does reflect the necessary qualitative features of the dynamics. Of the remaining sites in Figure 2, site 4 was seen to have the largest impact on the population relaxation. Calculations that consist of pathway 1 plus site 4 shown in Figure 3a are seen to capture almost all of the behavior seen in the full eight-site system. Increasing the trapping rate at site 3 decreases the differences seen between the trapping times of the four- and five-site models.

In ref 15, it was noted that the site energy of Bchl 8 maximizes the overlap with the chlorosome emission spectrum while simultaneously maintaining a large energy gap with the remaining seven core Bchls. This indicates that there should be an optimal value of the site energy of Bchl 8. In addition to the observation that the trapping time behavior may be captured by a simplified model of FMO, there is another interesting feature seen in Figure 3. The trapping time displays a minimum as a function of the energy of the eighth site for all of the constructed models. Moreover, for the eight-site model, the optimal value of the site energy is rather close to the fitted value of 505 cm^{-1}.[15] Increasing the energy difference between site 8 and site 1 decreases the back-transfer rate but also decreases the spectral overlap between the two. The position of the optimal value is no coincidence. The three-site model in Figure 1c readily demonstrates that this particular choice for the site energy leads to a

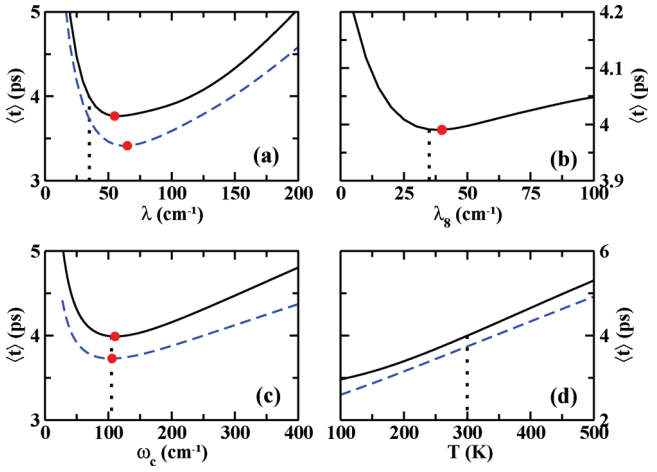

Figure 4. The trapping time as a function of the reorganization energy of all Bchls (a) and as a function of the reorganization of site 8 only (b) while the remaining seven sites are fixed at the experimentally fitted value of $\lambda = 35\ cm^{-1}$. The trapping time as a function of the bath cutoff frequency and temperature are shown in (c) and (d), respectively. In all cases, the trap rate at site 3 is 1 ps. The solid (black) and dashed (blue) lines correspond to initial excitation at site 8 and site 1, respectively. The red dots indicate the optimal trapping times, and the dotted vertical lines correspond to the respective experimentally fitted values. The remaining parameters are the same as those in Figure 2.

downhill configuration of three sites that are approximately equally spaced and equally coupled. The impact of the geometry of the system on the energy-transfer properties of excitonic systems has been analyzed in detail in ref 18. There it was shown that this configuration is among the most favorable. The qualitative behavior of the trapping time in the full, complicated eight-site system becomes obvious with the aid of the reduced models. Note also that the average trapping time varies little over a large range of values of the energy of site 8, indicating the robustness of the energy-transfer process. Below, it is demonstrated that many of the other fitted parameters are near-optimal as well.

Optimal Bath Parameters. The average trapping time calculated as a function of the reorganization energy is shown in Figures 4a and b. Figure 4a varies the reorganization energy of all eight sites simultaneously (in this model, all chromophores are assumed to have identical environments), whereas Figure 4b varies only that of site 8 while keeping all of the others at the fitted value of 35 cm^{-1}. In order to demonstrate that the presence of the additional chromophore does not lead to a dramatic increase in the trapping time, two different initial conditions are taken with either site 1 or site 8 initially excited. As expected, a slightly larger trapping time is observed with the initial population at site 8 due to the larger distance to the trap. However, the difference between the two scenarios is not substantial. Additionally, the qualitative behavior of the two initial conditions is quite similar, and both lead to an optimal value of the reorganization energy that is close to the experimentally fitted value of 35 cm^{-1}. It has been proposed from recent numerical simulations that the reorganization energy in FMO should be approximately twice as large as the experimentally fitted value used here.[36] The optimal values of λ in Figure 4a (55 cm^{-1}) and b (40 cm^{-1}) are consistent with a somewhat larger value of the reorganization energy. Note however the difference in the scales of the average trapping time in Figures 4a and b. While the optimal value in Figure 4b is closer to the experimentally fitted value, the average trapping time is larger than the corresponding values in Figure 4a. Additionally, the results in Figure 4a display a much greater sensitivity to the reoganization energy than those in Figure 4b. The mean trapping time is more sensitive to variations of the reorganization energy than was observed for the site energy in Figure 3, but there is still a large range of λ where the trapping time is near-optimal.

Finally, Figures 4c and d displays the results for the average trapping time calculated as a function of the Debye frequency and as a function of the temperature. As in Figure 4a, two initial conditions are shown with the initial population at either site 1 or site 8. Again, the average trapping time from site 1 is always faster than that for site 8. Nevertheless, the two initial conditions display qualitatively similar behavior for both the temperature and Debye frequency. Additionally, an optimal value of the Debye frequency is observed that is close to the experimentally fitted value of 105 cm^{-1}. The increase in the trapping time with increasing temperature has also been observed in the first paper of this series.[11] It is a consequence of the fact that increasing the temperature in a purely downhill setting leads to a corresponding increase of the back-transfer rate away from the trap. In general, the results in Figure 4 for the average trapping time as a function of the bath parameters are similar to those observed previously for the seven-site model of FMO.[11] There is one notable difference however. In all cases, the Hamiltonian for the eight-site FMO model recently proposed by Renger et al.[15] leads to optimal conditions that are closer to the experimentally fitted values than those calculated previously[11] using the Hamiltonian of ref 28.

The FMO protein serves as one of the model light-harvesting systems, and the qualitative features of the energy-transfer process have been understood for some time. However, recent experimental evidence has shown that many of the previously developed theoretical models are not entirely complete. An additional chromophore is present in each subunit of FMO that resides between the chlorosome and site 1. In this work, we have shown that the presence of the eighth site does not significantly alter the previous conclusions that have been reached with regards to environmentally assisted exciton transport.[11] Optimal values exist for many of the bath parameters, and moreover, the optimal conditions are generally closer to their respective experimentally fitted values than those in the seven-site FMO models. Additionally, the dependence of the average trapping time with respect to variations of the bath parameters is rather weak, illustrating the overall robustness of the energy-transfer process.

However, the presence of the eighth Bchl may necessitate a reassessment of our understanding of the energy-transport process in FMO. Given that site 8 is the primary entry point for the exciton into FMO, Figure 2 clearly exhibits a complete suppression of the population oscillations that are generally observed in the seven-site models of FMO. That is, the coherent population oscillations observed in previous studies depend on the special choice of initial conditions. Here, we have shown that the origin of the suppression is the slow decay of the initial population at site 8, which leads to an incoherent distribution of initial conditions at the dimer. In the physical setting, there will be an additional source of dephasing due to the extra step from the chlorosome to FMO. This will broaden the distribution of initial conditions even more and further suppress the oscillations in the dimer.

An additional feature of the eight-site model that is markedly different from the previous seven-site configuration is observed in the population dynamics shown in Figure 2 and the average trapping times displayed in Figure 3. These results demonstrate that the energy flow in the eight-site model is dominated by a subset of the chromophores, whereas it has been previously assumed that two independent pathways involving all of the Bchls are available for the energy-transfer process. The qualitative features of the transport in the eight-site model are largely determined by the dynamics of pathway 1. Sites 4, 5, 6, and 7 provide a rather small contribution to the overall efficiency in this case. The agreement between the results for the full eight-site system and those for the reduced four- and three-site models shown in Figure 1 provide further support to this claim. Nevertheless, the eight-site model and the seven-site model display similar energy-transport efficiencies. The origin of this behavior in the former is evident from Figure 1c, which shows that the eighth Bchl forms an optimal downhill ladder configuration with the dimer and site 3.[18] This result demonstrates the usefulness of the reduced models in providing an intuitive explanation of many of the key features present in the numerical results.

■ ASSOCIATED CONTENT

Supporting Information. The Supporting Information contains the explicit form of the eight-site Hamiltonian for FMO used in the calculations.This material is available free of charge via the Internet at http://pubs.acs.org/.

■ AUTHOR INFORMATION

Corresponding Author
*E-mail: jianshu@mit.edu.

■ ACKNOWLEDGMENT

This work was supported by grants from the National Science Foundation (Grant Number CHE-1112825), DARPA (Grant Number N66001-10-1-4063), and the Singapore−MIT alliance for research and technology (SMART). JC is supported by the Center for Excitonics, an Energy Frontier Research Center funded by the US Department of Energy, Office of Basic Energy Sciences (Grant Number DE-SC0001088). DFC acknowledges support from the Science Foundation Ireland (SFI) Stokes Professors Program (Grant Number 07/SK/B1239b) and wishes to thank JC and SMART for hosting his visit to Singapore. JW acknowledges partial support from the Fundamental Research Funds for the Central Universities in China (Grant Number 2010QNA3041) and the National Science Foundation of China (Grant Number 21173185).

■ REFERENCES

(1) Fenna, R. E.; Matthews, B. W. Chlorophyll Arrangement in a Bacteriochlorophyll Protein from Chlorobium limicola. *Nature* **1975**, *258*, 573–577.

(2) Brixner, T.; Stenger, J.; Vaswani, H. M.; Cho, M.; Blankenship, R. E.; Fleming, G. R. Two-Dimensional Spectroscopy of Electronic Couplings in Photosynthesis. *Nature* **2005**, *434*, 625–628.

(3) Engel, G. S.; Calhoun, T. R.; Read, E. L.; Ahn, T.; Mancal, T.; Cheng, Y.; Blankenship, R. E.; Fleming, G. R. Evidence for Wavelike Energy Transfer through Quantum Coherence in Photosynthetic Systems. *Nature* **2007**, *446*, 782–786.

(4) Panitchayangkoon, G.; Hayes, D.; Fransted, K. A.; Caram, J. R.; Harel, E.; Wen, J.; Blankenship, R. E.; Engel, G. S. Long-Lived Quantum Coherence in Photosynthetic Complexes at Physiological Temperature. *Proc. Natl. Acad. Sci. U.S.A.* **2010**, *107*, 12766–12770.

(5) Collini, E.; Wong, C. Y.; Wilk, K. E.; Curmi, P. M. G.; Brumer, P.; Scholes, G. D. Coherently Wired Light-Harvesting in Photosynthetic Marine Algae at Ambient Temperature. *Nature* **2010**, *463*, 644–647.

(6) Ben-Shem, A.; Frolow, F.; Nelson, N. Evolution of Photosystem I — From Symmetry Through Pseudosymmetry to Asymmetry. *FEBS Lett.* **2004**, *564*, 274–280.

(7) Tronrud, D. E.; Wen, J.; Gay, L.; Blankenship, R. E. The Structural Basis for the Difference in Absorbance Spectra for the FMO Antenna Protein from Various Green Sulfur Bacteria. *Photosynth. Res.* **2009**, *100*, 79–87.

(8) Ishizaki, A.; Fleming, G. R. Unified Treatment of Quantum Coherent and Incoherent Hopping Dynamics in Electronic Energy Transfer: Reduced Hierarchy Equation Approach. *J. Chem. Phys.* **2009**, *130*, 234111.

(9) Huo, P.; Coker, D. F. Iterative Linearized Density Matrix Propagation for Modeling Coherent Excitation Energy Transfer in Photosynthetic Light Harvesting. *J. Chem. Phys.* **2010**, *133*, 184108.

(10) Tao, G.; Miller, W. H. Semiclassical Description of Electronic Excitation Population Transfer in a Model Photosynthetic System. *J. Phys. Chem. Lett.* **2010**, *1*, 891–894.

(11) Wu, J.; Liu, F.; Shen, Y.; Cao, J.; Silbey, R. J. Efficient Energy Transfer in Light-Harvesting Systems, I: Optimal Temperature, Reorganization Energy and Spatial-Temporal Correlations. *New J. Phys.* **2010**, *12*, 105012.

(12) Hoyer, S.; Ishizaki, A.; Whaley, B. Propagating Quantum Coherence for a Biological Advantage. 2011, arXiv:1106:2911.

(13) Wu, J.; Liu, F.; Ma, J.; Wang, X.; Silbey, R.; Cao, J. Efficient Energy Transfer in Light-Harvesting Systems, II: Quantum-Classical Comparison, Flux Network, and Robustness Analysis. 2011, arXiv:1109.5769.

(14) Ishizaki, A.; Fleming, G. R. Theoretical Examination of Quantum Coherence in a Photosynthetic System at Physiological Temperature. *Proc. Natl. Acad. Sci. U.S.A.* **2009**, *106*, 17255–17260.

(15) Schmidt am Busch, M.; Müh, F.; Madjet, M. E.; Renger, T. The Eighth Bacteriochlorophyll Completes the Excitation Energy Funnel in the FMO Protein. *J. Phys. Chem. Lett.* **2011**, *2*, 93–98.

(16) Renaud, N.; Ratner, M. A.; Mujica, V. A Stochastic Surrogate Hamiltonian Approach of Coherent and Incoherent Exciton Transport in the Fenna−Matthews−Olson Complex. *J. Chem. Phys.* **2011**, *135*, 075102.

(17) Ritschel, G.; Roden, J.; Strunz, W. T.; Aspuru-Guzik, A.; Eisfeld, A. Suppression of Quantum Oscillations and Dependence on Site Energies in Electronic Excitation Transfer in the Fenna−Matthews−Olson Trimer. 2011, arXiv:1108.3452.

(18) Cao, J.; Silbey, R. J. Optimization of Exciton Trapping in Energy Transfer Processes. *J. Phys. Chem. A* **2009**, *113*, 13825–13838.

(19) Mohseni, M.; Rebentrost, P.; Lloyd, S.; Aspuru-Guzik, A. Environment-Assisted Quantum Walks in Photosynthetic Energy Transfer. *J. Chem. Phys.* **2008**, *129*, 174106.

(20) Plenio, M. B.; Huelga, S. F. Dephasing-Assisted Transport: Quantum Networks and Biomolecules. *New J. Phys.* **2008**, *10*, 113019.

(21) Chin, A. W.; Datta, A.; Caruso, F.; Huelga, S. F.; Plenio, M. B. Noise-Assisted Energy Transfer in Quantum Networks and Light-Harvesting Complexes. *New J. Phys.* **2010**, *12*, 065002.

(22) Daniels, G. J.; Andrews, D. L. The Electronic Influence of a Third Body onResonance Energy Transfer. *J. Chem. Phys.* **2002**, *116*, 6701.

(23) Mohseni, M.; Shabani, A.; Lloyd, S.; Rabitz, H. Optimal and Robust Energy Transport in Light-Harvesting Complexes: (II) A Quantum Interplay of Multichromophoric Geometries and Environmental Interactions. 2011, arXiv:1104.4812.

(24) Cao, J. A Phase-Space Study of Bloch-Redfield Theory. *J. Chem. Phys.* **1997**, *107*, 3204.

(25) Weiss, U. *Quantum Dissipative Systems*, 2nd ed.; World Scientific: Singapore, 1999.

(26) Mukamel, S. *Principles of Nonlinear Optical Spectroscopy*; Oxford University Press: New York, 1999.

(27) Pachon, L. A.; Brumer, P. The Physical Basis for Long-Lived Electronic Coherence in Photosynthetic Light Harvesting Systems. *J. Phys. Chem. Lett.* **2011**, *2*, 2728–2732.
(28) Cho, M.; Vaswani, H. M.; Brixner, T.; Stenger, J.; Fleming, G. R. Exciton Analysis in 2D Electronic Spectroscopy. *J. Phys. Chem. B* **2005**, *109*, 10542–10556.
(29) Brumer, P.; Shapiro, M. Molecular Response in Coherent vs. Incoherent One Photon Absorption. 2011, arXiv:1109.0026.
(30) Silbey, R.; Harris, R. A. Variational Calculation of the Dynamics of a Two Level System Interacting with a Bath. *J. Chem. Phys.* **1984**, *80*, 2615.
(31) Aslangul, C.; Pottier, N.; Saint-James, D. Spin-Boson Systems: Equivalence Between the Dilute-Blip and the Born Approximations. *J. Phys. (Paris)* **1986**, *47*, 5.
(32) Cao, J. Effects of Bath Relaxation on Dissipative Two-State Dynamics. *J. Chem. Phys.* **2000**, *112*, 6719.
(33) Zwanzig, R. *Nonequilibrium Statistical Mechanics*; Oxford University Press: London, 2001.
(34) Kubo, R.; Toda, M.; Hashitsume, N. *Statistical Physics II: Nonequilibrium Statistical Mechanics*, 2nd ed.; Springer-Verlag: Berlin, Germany, 1985.
(35) Huo, P.; Coker, D. F. Theoretical Study of Coherent Excitation Energy Transfer in Cryptophyte Phycocyanin 645 at Physiological Temperature. *J. Phys. Chem. Lett.* **2011**, *2*, 825–833.
(36) Olbrich, C.; Strümpfer, J.; Schulten, K.; Kleinekathöfer, U. Theory and Simulation of the Environmental Effects on FMO Electronic Transitions. *J. Phys. Chem. Lett.* **2011**, *2*, 1771–1776.